Science Immunology
AAAS

Supplementary Materials for

Ikaros is a principal regulator of Aire^{+} mTEC homeostasis, thymic mimetic cell diversity, and central tolerance

Jun Hyung Sin *et al.*

Corresponding author: Michael R. Waterfield, michael.waterfield@ucsf.edu

Sci. Immunol. **8**, eabq3109 (2023)
DOI: 10.1126/sciimmunol.abq3109

The PDF file includes:

Other Supplementary Material for this manuscript includes the following:

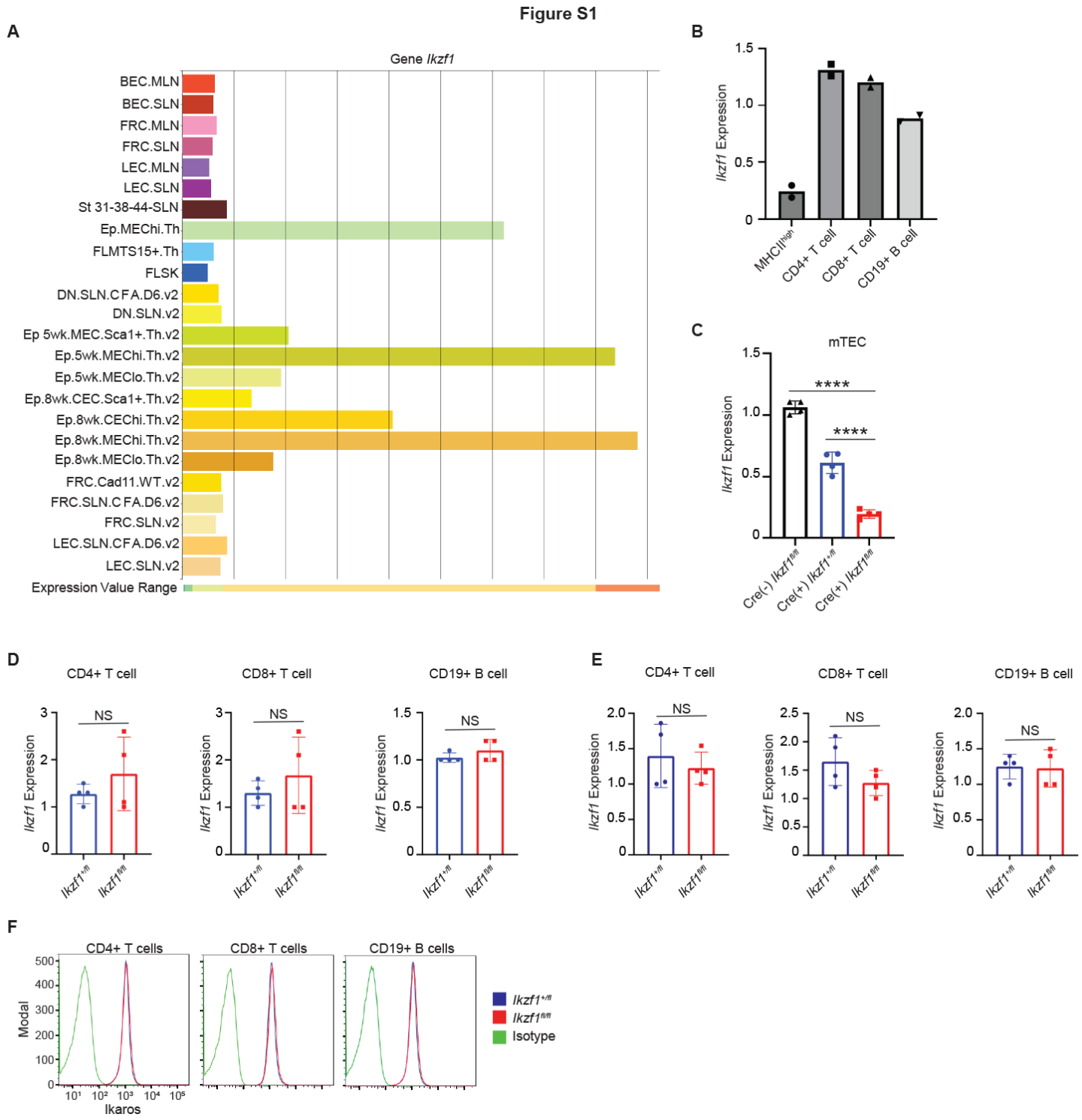

Fig. S1 – *Ikzf1* is efficiently deleted in *Foxn1*-Cre/*Ikzf1*$^{fl/fl}$ mTECs. (A) Relative expression of *Ikzf1* mRNA in stromal cells. Downloaded from the Immgen expression database. *Ikzf1* is highly expressed in medullary thymic epithelial cells (MEC^{hi}). **(B)** Relative expression of *Ikzf1* mRNA in sorted MHC-II^{high} mTECs and lymph node CD4$^+$ T cells, CD8$^+$ T cells, and CD19$^+$ B cells from C57BL/6 mice. **(C)** Relative expression of *Ikzf1* mRNA in sorted MHC-II^{high} mTECs from *Foxn1*-Cre(-)/*Ikzf1*$^{fl/fl}$, *Foxn1*-Cre(+)/*Ikzf1*$^{+/fl}$, and *Foxn1*-Cre(+)/*Ikzf1*$^{fl/fl}$ mice. (n = 4 mice per genotype). **(D)** Relative expression of *Ikzf1* mRNA in sorted lymph node CD4$^+$ T cells, CD8$^+$ T cells, and CD19$^+$ B cells from *Foxn1*-Cre/*Ikzf1*$^{fl/fl}$ (*Ikzf1*$^{fl/fl}$) and *Foxn1*-Cre/*Ikzf1*$^{+/fl}$ (*Ikzf1*$^{+/fl}$) mice. (n = 4 mice per genotype). **(E)** Relative expression of *Ikzf1* mRNA in sorted splenic CD4$^+$ T cells, CD8$^+$ T cells, and CD19$^+$ B cells. (n = 4 mice per genotype). **(F)** Representative flow cytometry plots of Ikaros levels in splenic CD4$^+$ T cells, CD8$^+$ T cells and CD19$^+$ B cells. **(B-E)** In graphs, the bar corresponds to

the mean, with error bars showing +/- SD of values shown, and each data point represents an individual mouse. **(C)** Statistical significance was calculated using one-way ANOVA and grouped comparisons were corrected using Tukey's multiple-comparison test, ****P<0.0001. **(D, E)** Statistical significance was determined using Student's T-test. NS = not significant.

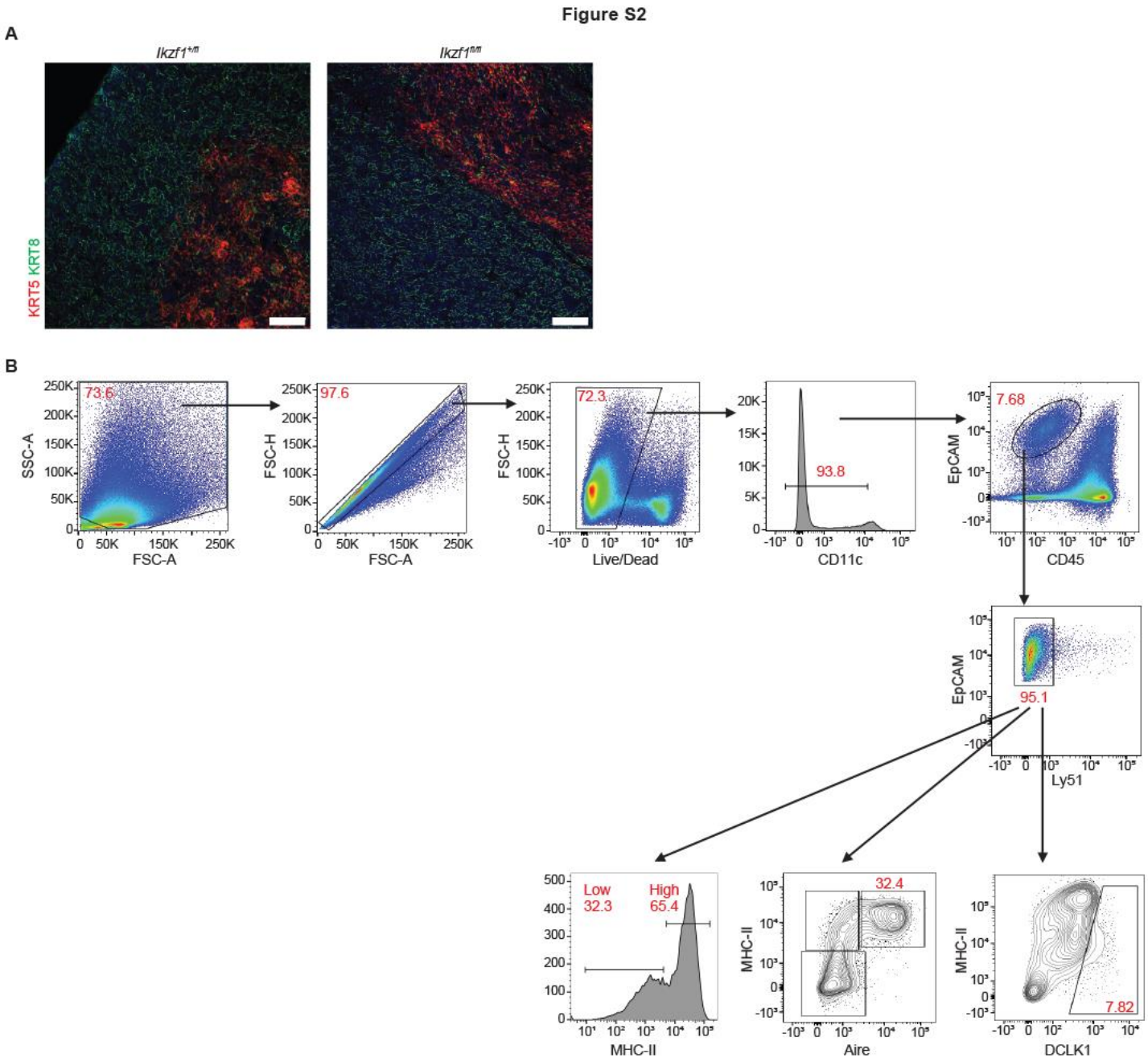

Fig. S2 – Deletion of *Ikzf1* does not alter thymic architecture. (A) Confocal microscopy of Keratin 5 (KRT5) (red) and Keratin 8 (KRT8) (green) of 30-day old thymi from *Foxn1*-Cre(+)/*Ikzf1*$^{+/fl}$ (*Ikzf1*$^{+/fl}$) mice and *Foxn1*-Cre(+)/*Ikzf1*$^{fl/fl}$ (*Ikzf1*$^{fl/fl}$) mice. Scale bars = 100 µm. **(B)** Flow cytometry gating strategy for the isolation CD11c^{-}EPCAM^{+} CD45^{-}LY51^{-}IA^{b+}Aire^{+} mTECs and CD11c^{-}EPCAM^{+} CD45^{-}LY51^{-}IA^{b+}DCLK1^{+} thymic tuft cells.

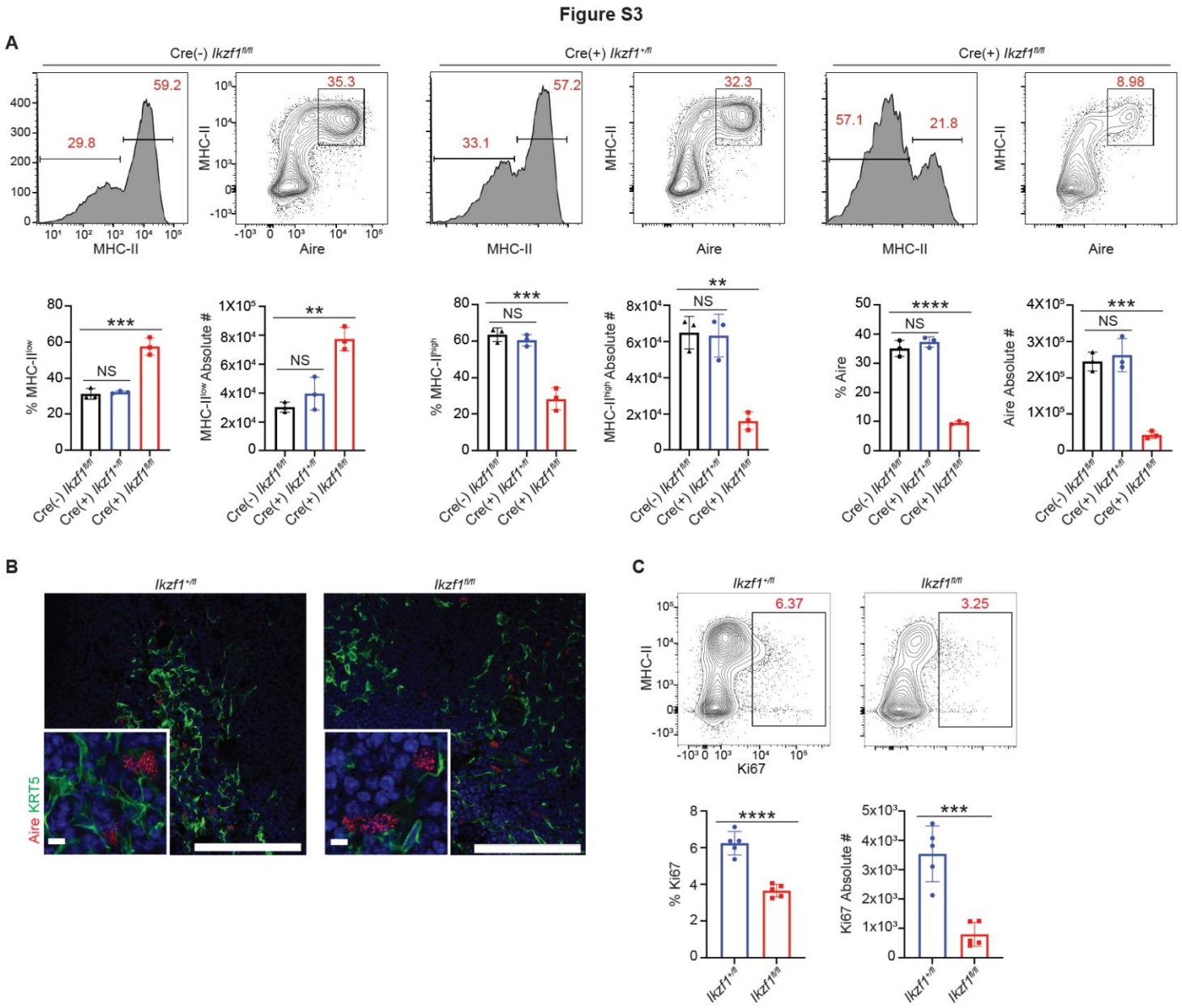

Fig. S3 – *Foxn1*-Cre(+)/*Ikzf1*$^{+/fl}$ and *Foxn1*-Cre(-)/*Ikzf1*$^{fl/fl}$ mice are phenotypically indistinguishable. (A) Flow cytometry (left) and percentage and absolute number (right) of CD11c^{-}EPCAM^{+}CD45^{-}LY51^{-}MHC-II^{high}, MHC-II^{low}, and Aire^{+} mTECs from *Foxn1*-Cre(-)/*Ikzf1*$^{fl/fl}$ mice, *Foxn1*-Cre(+)/*Ikzf1*$^{+/fl}$ mice, and *Foxn1*-Cre(+)/*Ikzf1*$^{fl/fl}$ mice. (n = 3 mice per genotype). **(B)** Confocal microscopy of Aire (red) and KRT5 (green) from 30-day old thymi. Scale bars = 100 µm and 20 µm for inset. **(C)** Flow cytometry (left) and percentage and absolute number (right) of CD11c^{-}EPCAM^{+} CD45^{-}LY51^{-}IA^{b+}Ki67^{+} mTECs. (n = 5 mice per genotype). **(A and C)** In graphs, the bar corresponds to the mean, with error bars showing +/- SD of values shown, and each data point represents an individual mouse. **(A)** Statistical significance was calculated using one-way ANOVA and grouped comparisons were corrected using Tukey's multiple-comparison test, **P<0.01, ***P<0.001, ****P<0.0001. NS = not significant. **(C)** Statistical significance was determined using Student's T-test, *** P<0.001, **** P<0.0001.

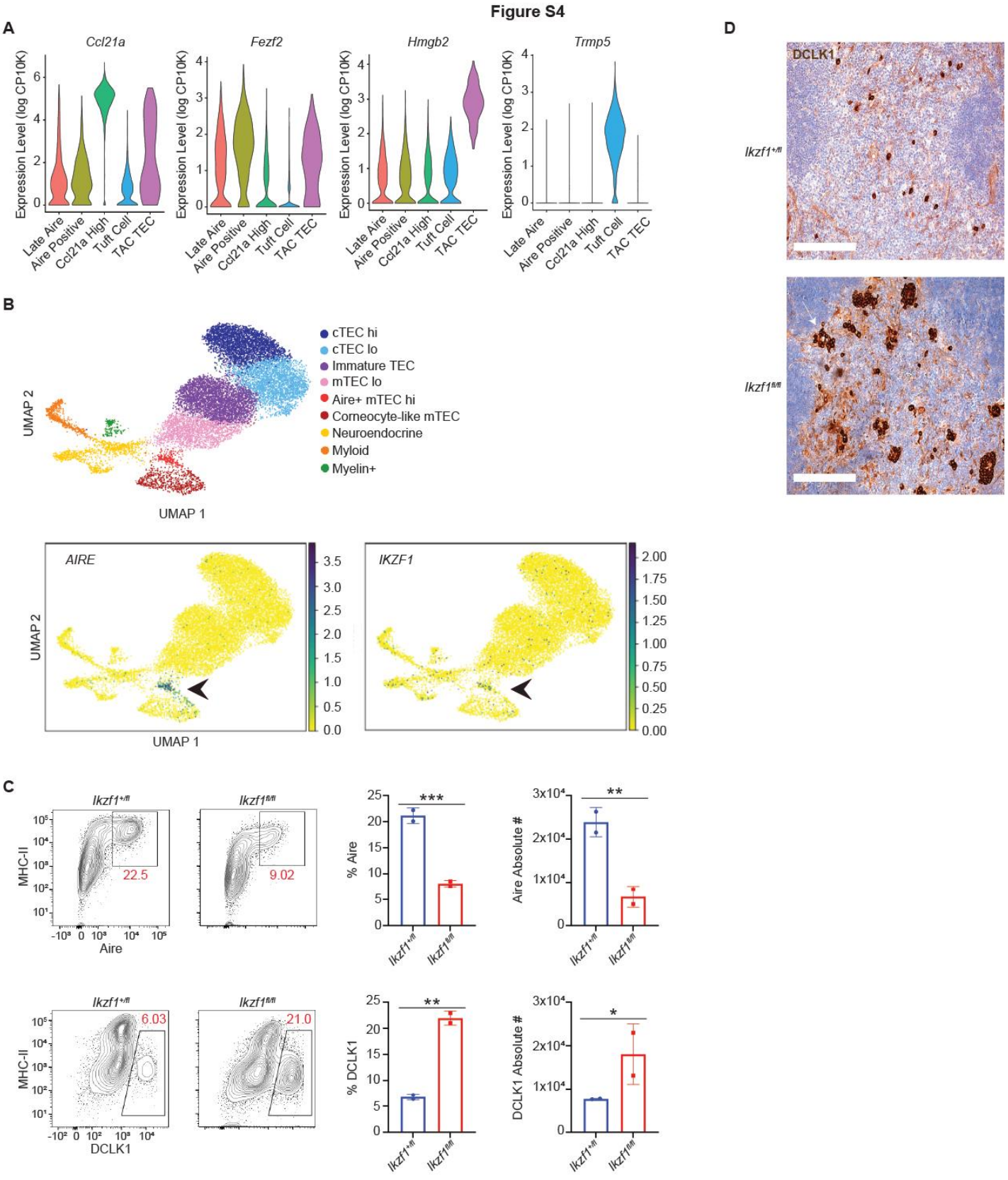

Fig. S4 – *IKZF1* is present in human mTECs. (A) Violin plots of marker genes for specific mTEC subsets from murine scRNA-seq data. **(B)** UMAPs of scRNA-seq data from human thymic epithelial cells. Arrows denote the mTEC subset with increased *AIRE* and *IKZF1* expression. **(C)** Flow cytometry (left) and percentage and absolute number of $CD11c^{-}EPCAM^{+}CD45^{-}LY51^{-}Aire^{+}$ and $DCLK1^{+}$ mTECs in 6-month-old *Foxn1*-Cre/*Ikzf1*$^{+/fl}$ mice and *Foxn1*-Cre/*Ikzf1*$^{fl/fl}$ mice. (n = 2 mice per genotype). **(D)** Representative

immunohistochemistry images of 30- day-old thymi stained with DCLK1 (5 µm sections). Scale Bar = 100 µm. **(C)** In graphs, the bar corresponds to the mean, with error bars showing +/- SD of values shown, and each data point represents an individual mouse. **(C)** Statistical significance was determined using Student's T-test. *P<0.05, **P<0.01, ***P<0.001.

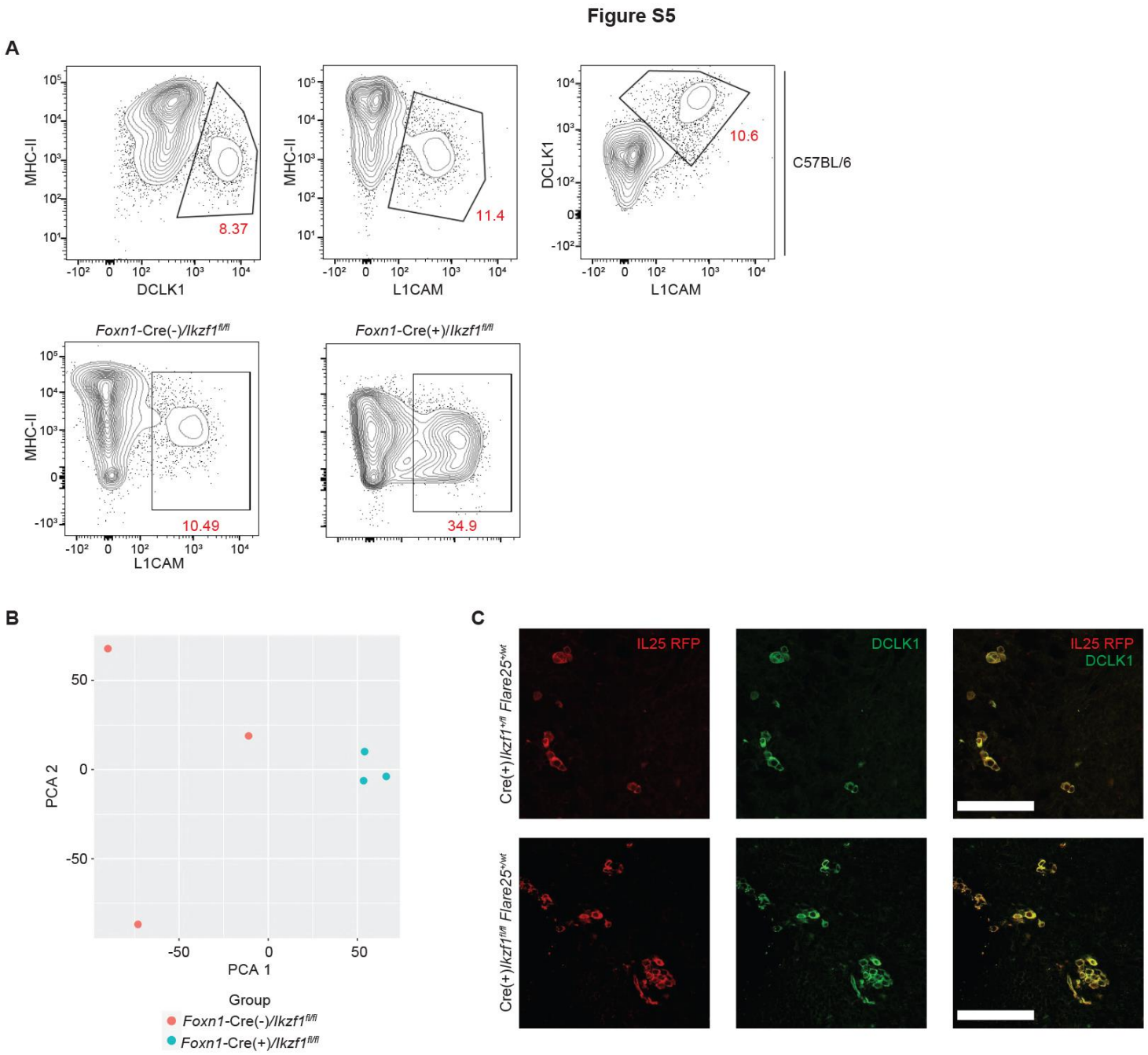

Fig. S5 – Expression of DCLK1 and IL-25 overlap in tuft cells. **(A)** Flow cytometry of CD11c^{-}EPCAM^{+} CD45^{-}LY51^{-}DCLK1^{+} and CD11c^{-}EPCAM^{+}CD45^{-}LY51^{-}L1CAM^{+} tuft cells in C57BL/6, *Foxn1*-Cre(-)/*Ikzf1*$^{fl/fl}$, and *Foxn1*-Cre(+)/*Ikzf1*$^{fl/fl}$ mice. **(B)** Principal component analysis of bulk RNA-seq data from sorted L1CAM^{+} tuft cells. Each data point represents tuft cells isolated from an individual mouse. **(C)** Representative confocal images (25 µm sections) of IL25-RFP (red) and DCLK1 (green) from 30-day old thymi of the indicated genotype. Immunofluorescence (IF) staining of thymic slices at high (40X optical) magnification. Scale bars = 100 µm.

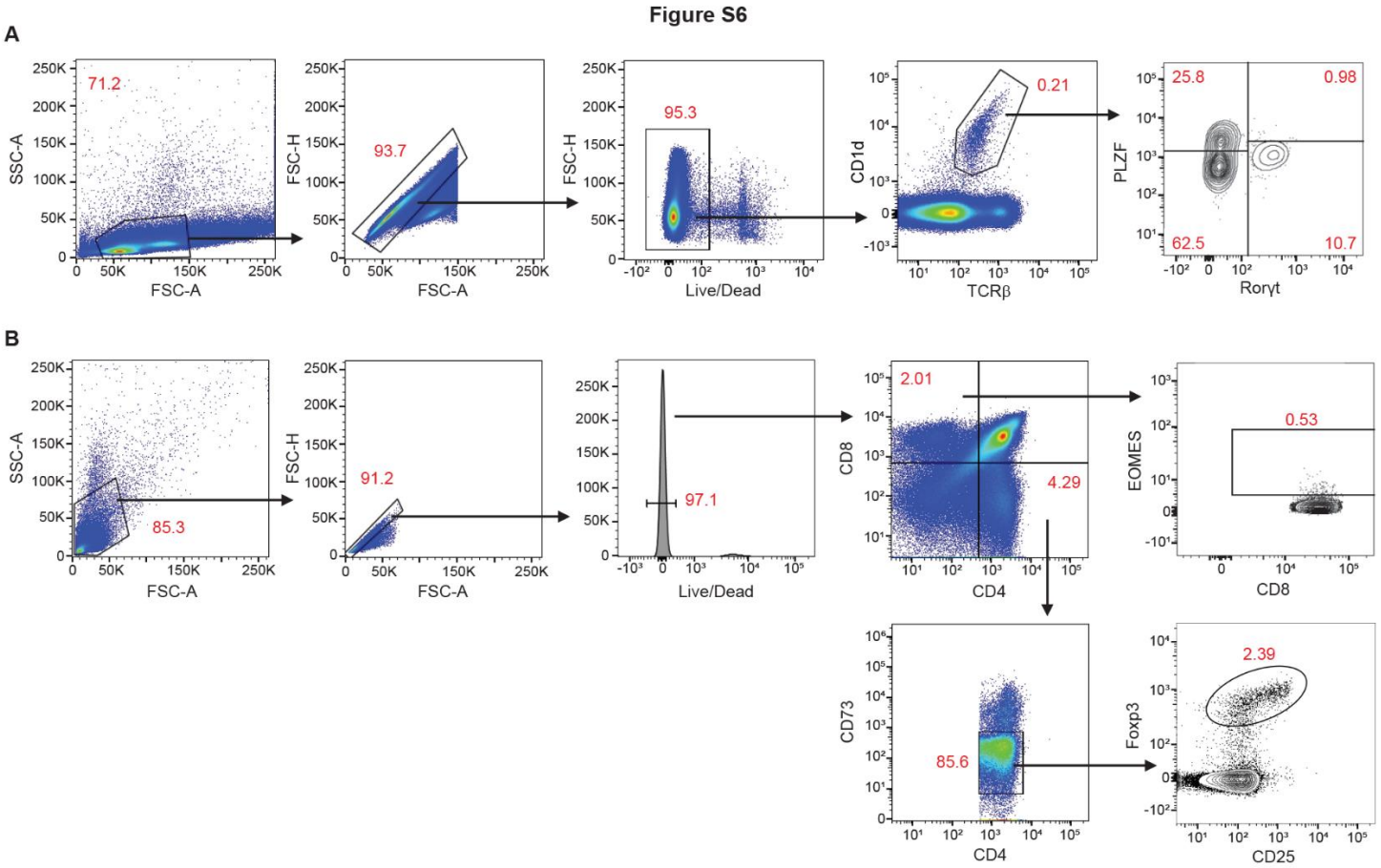

Fig. S6 – Gating strategy for iNKT and CD8$^+$ EOMES panels. **(A)** Representative flow cytometry gating strategy for two iNKT subsets: CD1d$^+$PLZF1$^+$ iNKT2s and CD1d$^+$RORγt$^+$ iNKT3s. **(B)** Representative flow cytometry gating strategy for CD8$^+$EOMES$^+$ innate T cells and CD4$^+$CD73$^-$CD25$^+$Foxp3$^+$ Tregs.

Figure S7

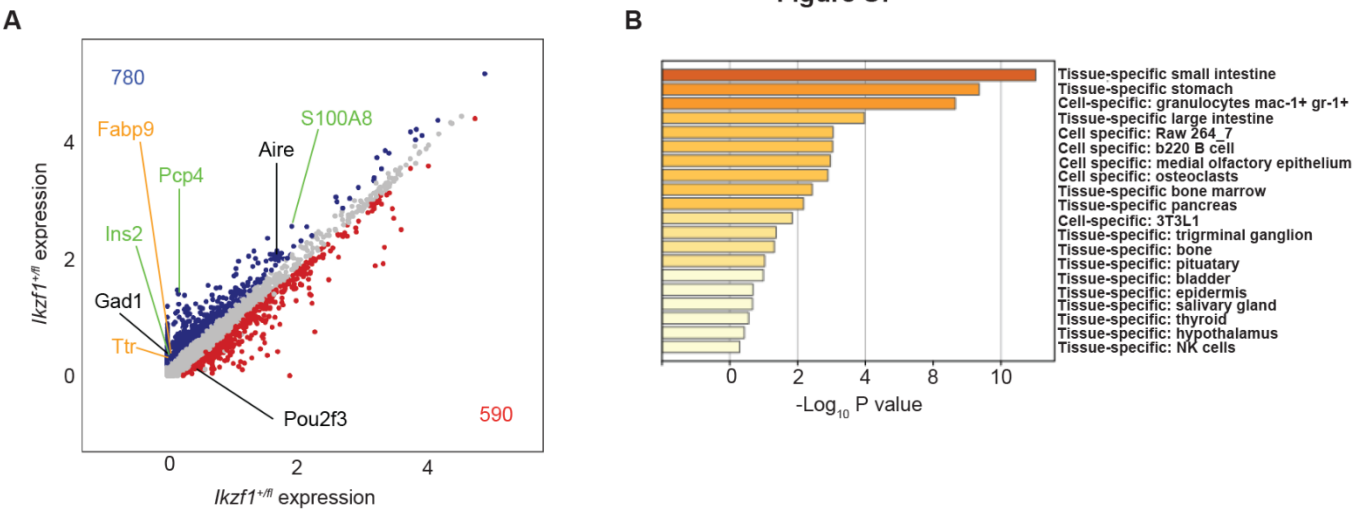

C

Gene Name	Gene Symbol	Log2Fold Change	Adj p-value	p-value	Tissues
Mucl2	Mucin-like 2	1.913297352	0.529669527	3.47E-05	Salivary gland, lacrimal gland
Pcp4	Purkinje cell protein 4	1.797459199	2.34E-09	1.53E-13	Nervous system
Mt4	Metallothionein	1.73416747	5.21E-05	3.41E-09	Stomach, epidermis
Nts	Neurotensin	1.622555936	0.000922221	6.04E-08	CNS, small intestine
Ccl20	Chemokine ligand 20	1.533744099	0.000111574	7.31E-09	Intestine
Prss29	Protease, serine 29	1.457943407	5.58E-06	3.66E-10	Pancreas, liver
Cck	Cholecystokinin	1.380825312	1	0.000968302	CNS, small intestine
Psors1c2	Psoriasis susceptibility 1 candidate 2	1.379490195	5.87E-17	3.85E-21	Stomach
Hspb1	Heat shock protein 1	1.344302414	0.000514528	3.37E-08	Multiple tissues
Serpinb12	Serine peptidase inhibitor, clade B, member 12	1.29719266	6.38E-12	4.18E-16	Stomach
Camp	Cathelicidin antimicrobial peptide	1.295053433	0.029201447	1.91E-06	Bone, bone marrow
Fam25c	Family with sequence similarity 25, member C	1.274812548	0.003705061	2.43E-07	Epidermis
Avp	Arginine vasopressin	1.273876859	0.049323997	3.23E-06	Hypothalamus
S100a9	S100 calcium binding protein A9	1.266993373	1.30E-11	8.50E-16	Bone, bone marrow
Retnla	Resistin like alpha	1.213130905	0.002056968	1.35E-07	Adipose
Ncf1	Neutrophil cytosolic factor 1	1.198249572	1.55E-30	1.01E-34	Macrophage, bone marrow
Gdf15	Growth differentiation factor 15	1.19522158	9.12E-19	5.97E-23	Macrophage, mast cells
Lyz2	Lysozyme 2	1.195178132	2.77E-19	1.82E-23	Lung, bone marrow
Ppy	Pancreatic polypeptide	1.179043297	0.006834122	4.48E-07	Pancrease, adipose
Tkt	Transketolase	1.175051931	1.80E-38	1.18E-42	Adipose, eye
Rarres1	Retinoic acid receptor responder 1	1.169588396	5.86E-08	3.84E-12	Epidermis, liver
Calcb	Calcitonin-related polypeptide, beta	1.166937573	8.92E-28	5.84E-32	Dorsal root ganglia
Sprr1a	Small proline-rich protein 1A	1.166560782	3.29E-13	2.15E-17	Bladder, stomach, uterus
Mucl1	Mucin-like 1	1.161735084	1	8.81E-05	Salivary gland, lacrimal gland
Igfbp6	Insulin-like growth factor binding protein 6	1.148535402	9.26E-05	6.07E-09	Multiple tissues

Aire Dependent TSA
Fezf2 Dependent TSA
Aire/Fezf2 Independent TSA
Non-TSA

Fig. S7 – scRNA-seq reveals that *Ikzf1*-deletion results in decreased TSA gene expression. (A) Gene expression in *Foxn1*-Cre/*Ikzf1*$^{+/fl}$ mice (*Ikzf1*$^{+/fl}$) versus *Foxn1*-Cre/*Ikzf1*$^{fl/fl}$ mice (*Ikzf1*$^{fl/fl}$) in Aire^{+} mTECs. Blue numbers represent the number of genes increased in *Ikzf1*$^{+/fl}$ mTECs (log2FC>0.25, p<0.05) and red numbers equal the number of genes increased *Ikzf1*$^{fl/fl}$ mTECs (log2FC>0.25, p<0.05). Genes labelled in green are Aire-dependent TSAs and genes labelled in orange are Fezf2-dependent TSA genes. **(B)** Metascape gene ontology analysis showing pathways downregulated in *Foxn1*-Cre/*Ikzf1*$^{fl/fl}$ Aire^{+} mTECs. **(C)** Table of top 25 genes downregulated in *Ikzf1*$^{fl/fl}$ Aire^{+} mTECs.

Figure S8

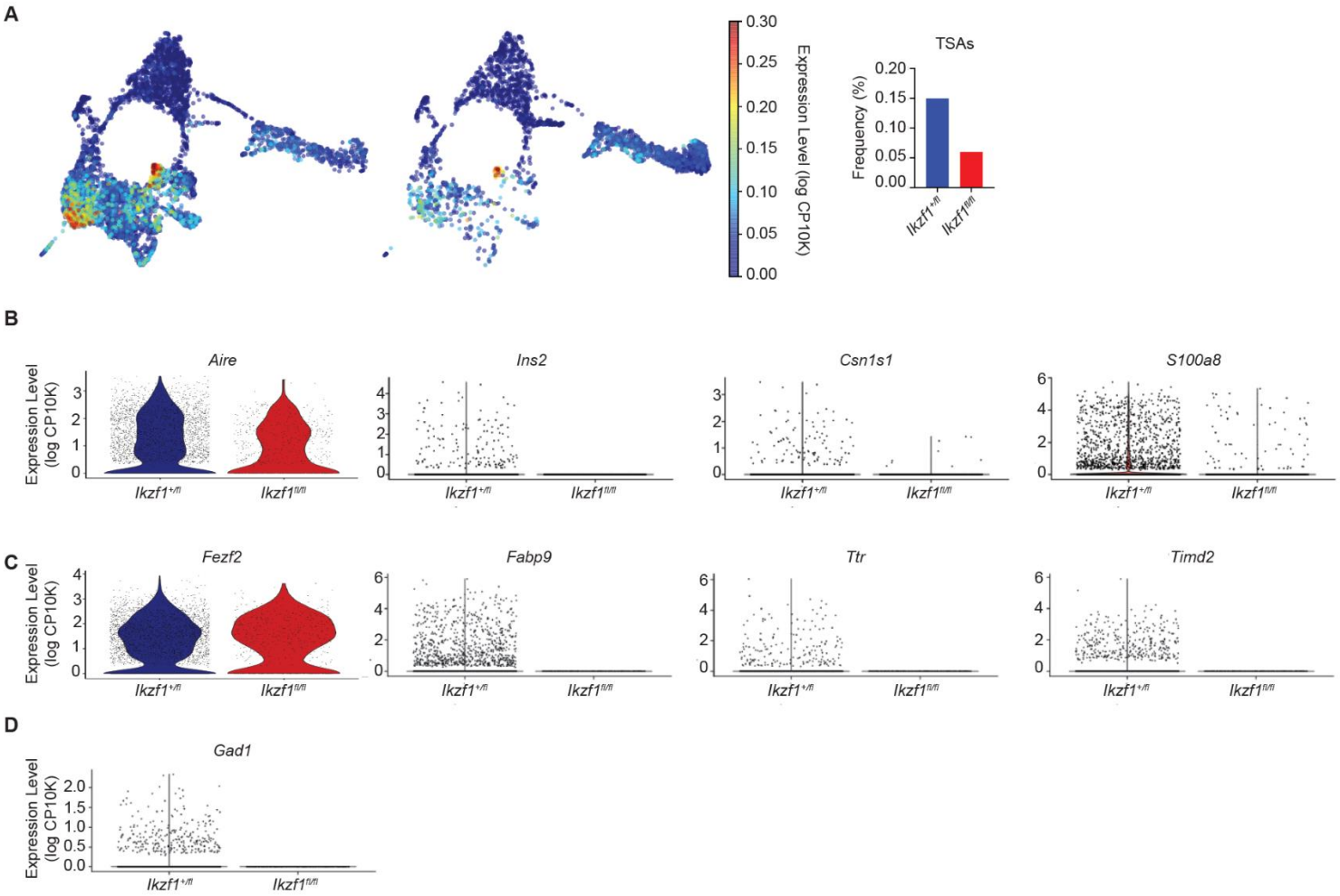

Fig. S8 – Ikaros regulates TSA gene expression. (A) UMAP visualization of the average expression of TSA genes. Bar graph shows the percentage of Aire^{+} mTECs expressing TSA genes at an expression level of 0.15. **(B)** Violin plots for Aire and Aire-dependent TSA genes in Aire^{+} mTECs. **(C)** Violin plots for Fezf2 and Fezf2-dependent TSA genes in Aire^{+} mTECs. **(D)** Violin plot for the Aire/Fezf2-independent TSA gene *Gad1* in Aire^{+} mTECs.

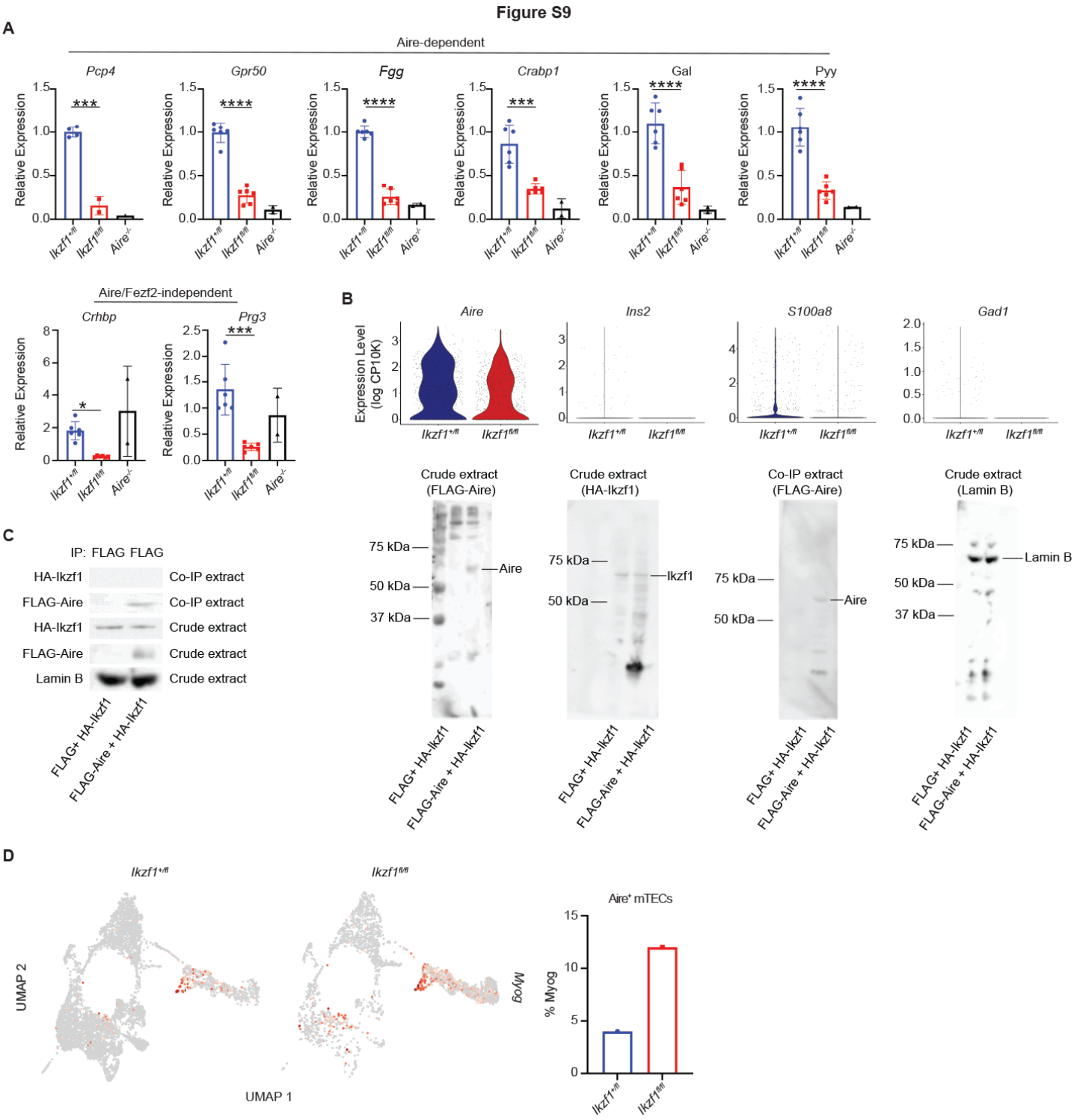

Fig. S9 – Ikaros modulates TSA gene expression and Ikaros does not interact with Aire. (A) qPCR of Aire-dependent and Aire/Fezf2-independent TSA gene expression. (n = 2 to 6 mice per genotype). **(B)** An equal number of Aire^{+} mTECs were analyzed (downsampling) to control for cell number(s) differences between genotypes. Violin plots are shown for Aire and the indicated TSA genes. **(C)** 293T cells were co-transfected with plasmids expressing either FLAG and HA-Ikzf1 or FLAG-Aire and HA-Ikzf1. Coimmunoprecipitation (Co-IP) was performed with an anti-FLAG antibody and proteins were visualized by western blot. **(D)** UMAP of *Myog* expression in Aire^{+} mTECs from scRNA-seq data. Bar graph represents the percentage of cells of each genotype expressing *Myog* in Aire^{+} mTECs. **(A)** In graphs, the bar corresponds to the mean, with error bars showing +/- SD of values shown, and each data point represents an individual mouse. **(A)** Statistical

significance was calculated using one-way ANOVA and grouped comparisons were corrected using Tukey's multiple-comparison test, *P<0.05, ***P<0.001, ****P<0.0001.

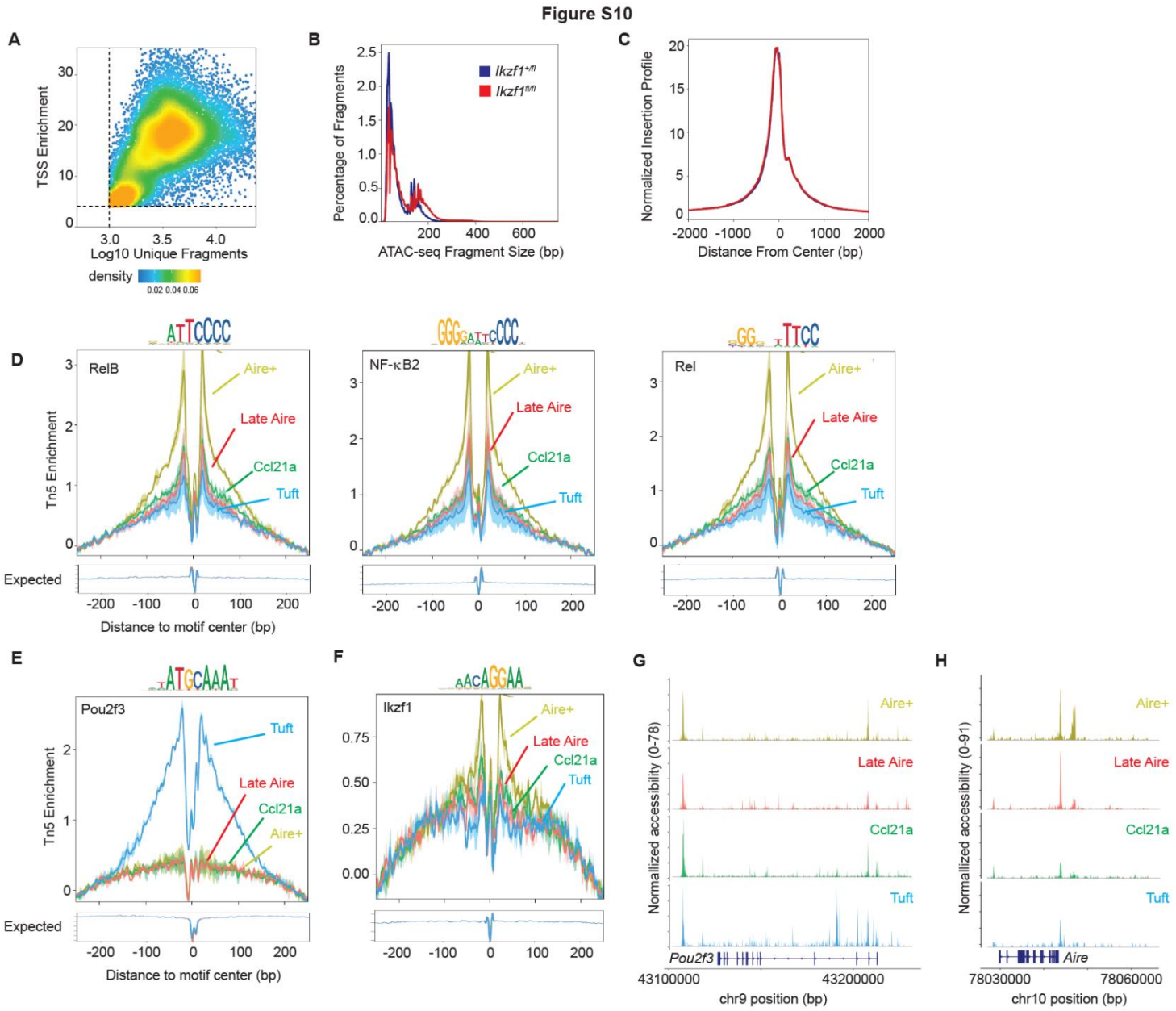

Fig. S10 – scATAC-seq identified four mTEC subsets: Aire^{+} mTECs, Late Aire mTECs, Ccl21a mTECs, and tuft cells. (A to C) scATAC-seq data quality control. **(A)** Number of unique nuclear fragments versus the transcriptional start site (TSS) enrichment of all fragments. **(B)** Percentage of fragments versus the ATAC-seq fragment size for each genotype (*Foxn1*-Cre/*Ikzf1*$^{+/fl}$ (*Ikzf1*$^{+/fl}$) versus *Foxn1*-Cre/*Ikzf1*$^{fl/fl}$ (*Ikzf1*$^{fl/fl}$) mTECs). **(C)** Normalized TSS enrichment score profile for each genotype. **(D to F)** TF footprints with motifs for each mTEC subset. Expected Tn5 insertion shown below. **(D)** TF footprints for select *NF-κB* family members, **(E)** *Pou2f3*, and **(F)** *Ikzf1*. **(G)** Genome track of pseudobulk scATAC-seq for the *Pou2f3* locus. **(H)** Genome track of pseudobulk scATAC-seq for the *Aire* locus.

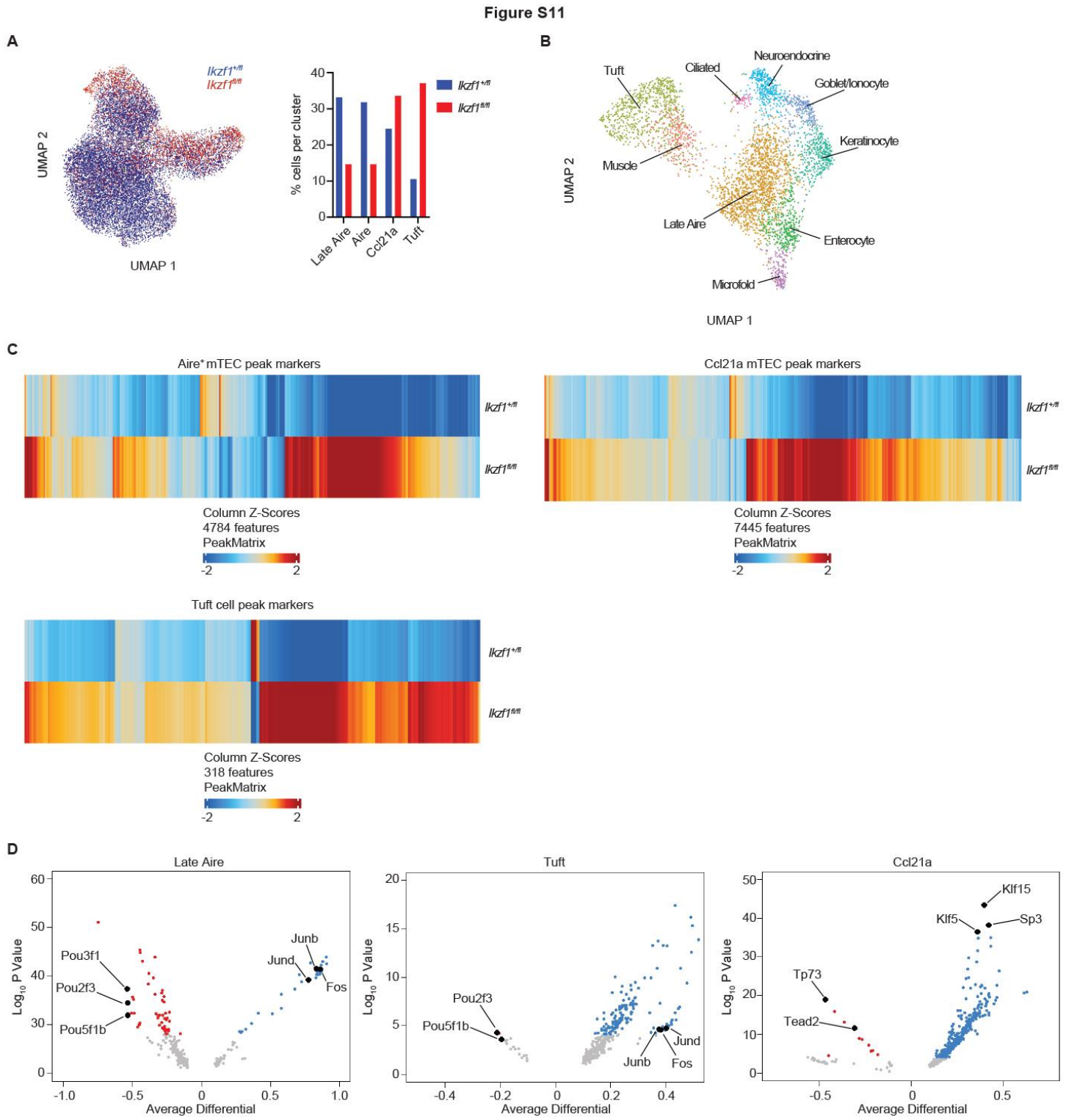

Fig. S11 - scATAC-seq replicates the cell composition changes seen in scRNA-seq. (A) UMAP of scATAC-seq clustering for the indicated genotypes. Blue = *Foxn1*-Cre/*Ikzf1*$^{+/fl}$ (*Ikzf1*$^{+/fl}$) mTECs and Red = *Foxn1*-Cre/*Ikzf1*$^{fl/fl}$ (*Ikzf1*$^{fl/fl}$) mTECs. Bar graph shows percentage of individual mTEC subsets for each genotype. **(B)** UMAP of mimetic cell populations within Late Aire and tuft scATAC-seq data. **(C)** Heat map of normalized scATAC-seq fragment density at differential peaks (FDR<0.05) for Aire^{+} mTECs, tuft cells, and Ccl21a mTECs. **(D)** chromVAR motif accessibility volcano plot in Late Aire mTECs, Ccl21a mTECs, and tuft cells. Blue dots show motifs significantly enriched (FDR <0.05) in *Foxn1*-Cre/*Ikzf1*$^{+/fl}$ (*Ikzf1*$^{+/fl}$) mTECs. Red dots show motifs significantly enriched in *Foxn1*-Cre/*Ikzf1*$^{fl/fl}$ (*Ikzf1*$^{fl/fl}$) mTECs (FDR <0.05).

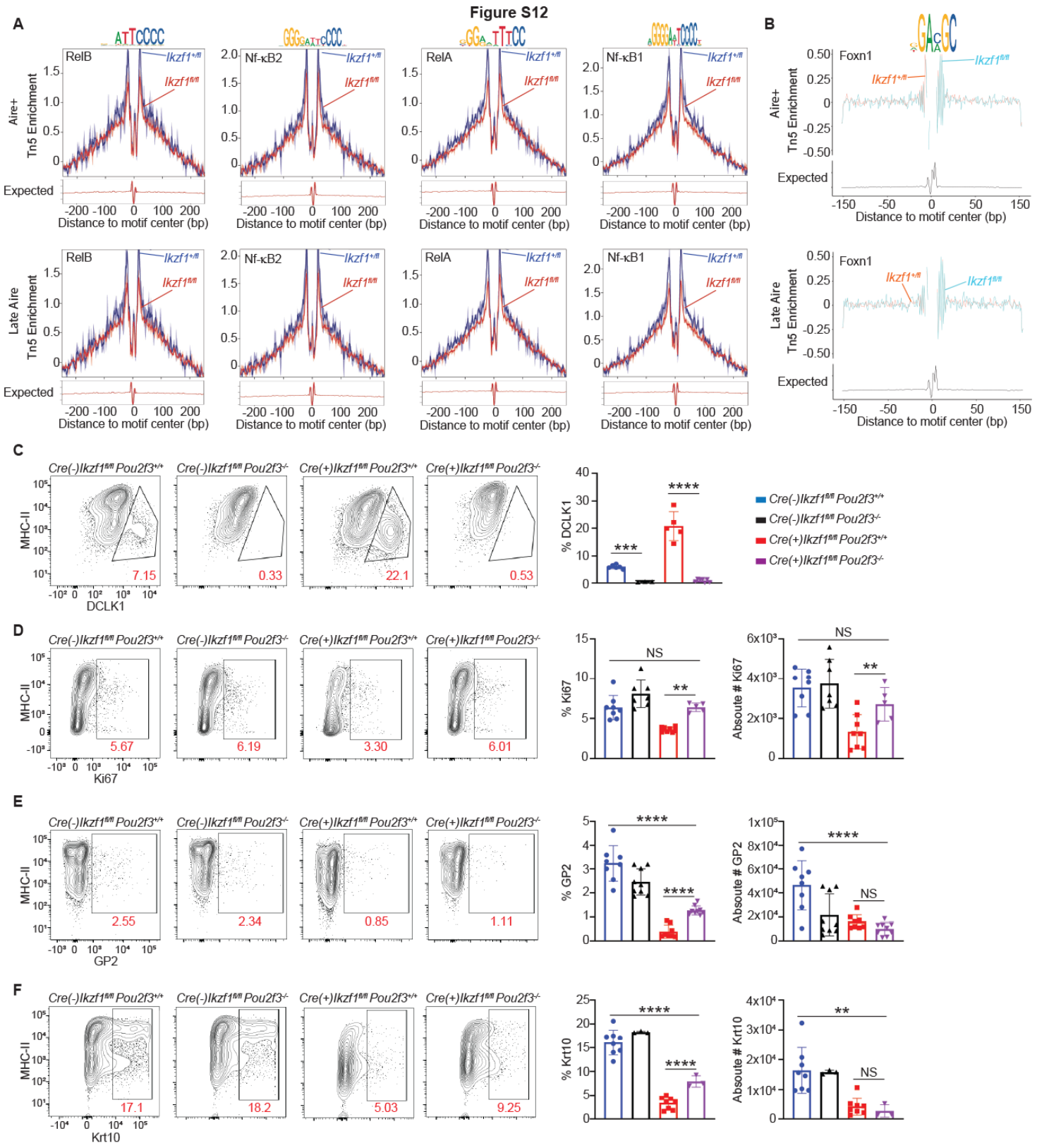

Fig. S12 - Combined deletion of *Ikzf1*/*Pou2f3* fails to rescue Aire-dependent mimetic cells. (A-B) TF footprints with motifs for *Foxn1*-Cre(+)/*Ikzf1*$^{+/fl}$ and *Foxn1*-Cre(+)/*Ikzf1*$^{fl/fl}$ Aire^{+} mTECs and Late Aire mTECs. Expected Tn5 insertion shown below. **(A)** TF footprints for select *NF-κB* family members, **(B)** *Foxn1*. **(C-F)** Flow cytometry (left) and percentage and absolute number (right) of mTEC populations from *Foxn1*-Cre(-)/*Ikzf1*$^{fl/fl}$/*Pou2f3*$^{+/+}$ mice, *Foxn1*-Cre(-)/*Ikzf1*$^{fl/fl}$/*Pou2f3*$^{-/-}$ mice, *Foxn1*-Cre(+)/*Ikzf1*$^{fl/fl}$/*Pou2f3*$^{+/+}$ mice, and *Foxn1*-Cre(+)/*Ikzf1*$^{fl/fl}$/*Pou2f3*$^{-/-}$ mice (n = 3-8 mice per genotype). **(C)** Staining for CD11c^{-}EPCAM^{+}CD45^{-}

$LY51^{-}IA^{b+}DCLK1^{+}$ tuft cells. **(D)** Staining for Ki67. **(E)** Staining for $GP2^{+}$ M cells. **(F)** Staining for $KRT10^{+}$ Keratinocytes. **(C-F)** In graphs, the bar corresponds to the mean, with error bars showing +/- SD of values shown, and each data point represents an individual mouse. **(C-F)** Statistical significance was calculated using one-way ANOVA and grouped comparisons were corrected using Tukey's multiple-comparison test, **P<0.01, ***P<0.001, ****P<0.0001. NS = not significant.

Figure S13

A

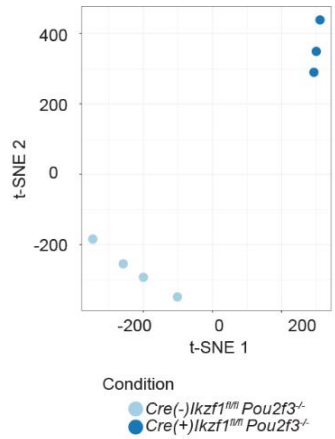

B

Gene Symbol	Gene Name	Log2 Fold Change	Adj p-value	p-value	Tissues
Stfa1	Stefin A1	9.865500921	1.99E-11	1.49E-13	Eye
Sprr2g	Small proline rich protein 2G	9.720099208	1.33E-12	7.61E-15	Lung, skeletal muscle
Lce1j	Late cornified envelope 1J	9.660912493	2.55E-12	1.56E-14	Liver
Defa29	Defensin, alpha, 29	9.472597139	2.65E-10	2.62E-12	Intestine
Ifnb1	Interferon beta 1	9.198989087	4.09E-09	5.57E-11	Salivary gland, T cells
Sprr2d	Small proline rich protein 2D	9.035133178	6.66E-10	7.53E-12	Uterus
Sprr2k	Small proline rich protein 2K	8.629837822	1.89E-09	2.39E-11	Uteurs
Prr9	Proline rich 9	8.593258683	3.85E-12	2.42E-14	Epidermis, testis
Crygc	Crystallin, gamma C	8.485894279	4.31E-09	5.95E-11	Eye
AY761185	Alpha-defensin propetide domain-containing protein	8.482133013	8.63E-09	1.29E-10	Testis
Spink13	Serine peptidase inhibitor kazal type 13	8.418019906	8.89E-09	1.34E-10	Blood vessel
Scgb3a2	Secretoglobin family 3A member 2	8.331433586	8.65E-09	1.30E-10	Lung
Obp1a	Odorant binding protein 1A	8.303068945	3.02E-08	5.25E-10	Lacrimal gland
Asb9	Ankyrin repeat and SOCS box containing 9	8.301809737	5.39E-09	7.61E-11	Testis, kidney
Cst11	Cystatin-11	8.267545423	2.74E-07	6.16E-09	Adipose
Crygs	Crystallin, gamma S	8.177974329	8.79E-11	7.46E-13	Eye
Retnlg	Resistin like gamma	8.141594896	0.003996433	0.000414601	Bone marrow, spleen
Defb37	Defensin beta 37	8.069424979	5.43E-08	1.00E-09	Multiple tissues
Stfa2l1	Stefin A2	8.029918561	3.14E-06	1.00E-07	Bone, granulocyte, bone marrow
Sprr2f	Small proline rich protein 2F	7.847854698	9.99E-11	8.63E-13	Uterus
Lce3a	Late cornified envelope 3A	7.796287729	1.20E-07	2.45E-09	Eye, stomach
Defa22	Defensin alpha 22	7.7659282	5.45E-07	1.32E-08	Intestine

■ Aire Dependent TSA ■ Fezf2 Dependent TSA □ Aire/Fezf2 Independent TSA ■ Non-TSA

C

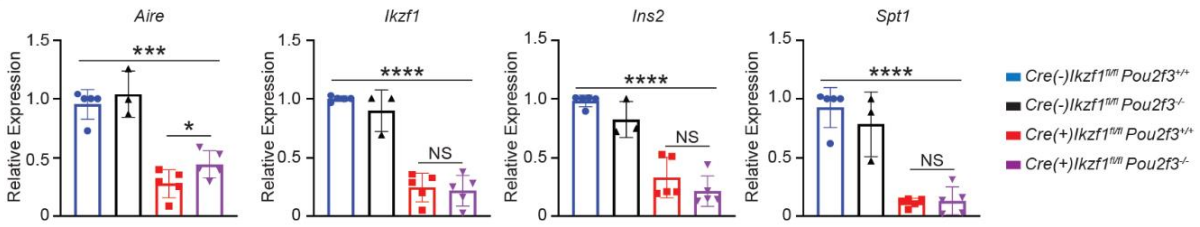

Fig. S13 - Bulk RNA-seq in MHC-II^{high} mTECs with combined *Ikzf1/Pou2f3* deletion. (A) t-distributed stochastic neighbor embedding (t-SNE) plot of bulk RNA-seq samples from MHC-II^{high} mTECs of the indicated genotype. Each data point represents MHC-II^{high} mTECs isolated from an individual mouse. **(B)** Table of top 25 genes upregulated genes in MHC-II^{high} mTECs in *Foxn1*-Cre(-)/*Ikzf1*$^{fl/fl}$/*Pou2f3*$^{-/-}$ versus *Foxn1*-Cre(+)/*Ikzf1*$^{fl/fl}$/*Pou2f3*$^{-/-}$. **(C)** qPCR of select target genes. Each data point represents an individual mouse. **(C)** In graphs, the bar corresponds to the mean, with the error bars showing +/- SD of values shown, and each data point represents an individual mouse. **(C)** Statistical significance was calculated using one-way ANOVA and grouped comparisons were corrected using Tukey's multiple-comparison test, *P<0.05, ***P<0.001, ****P<0.0001. NS = not significant.

Figure S14

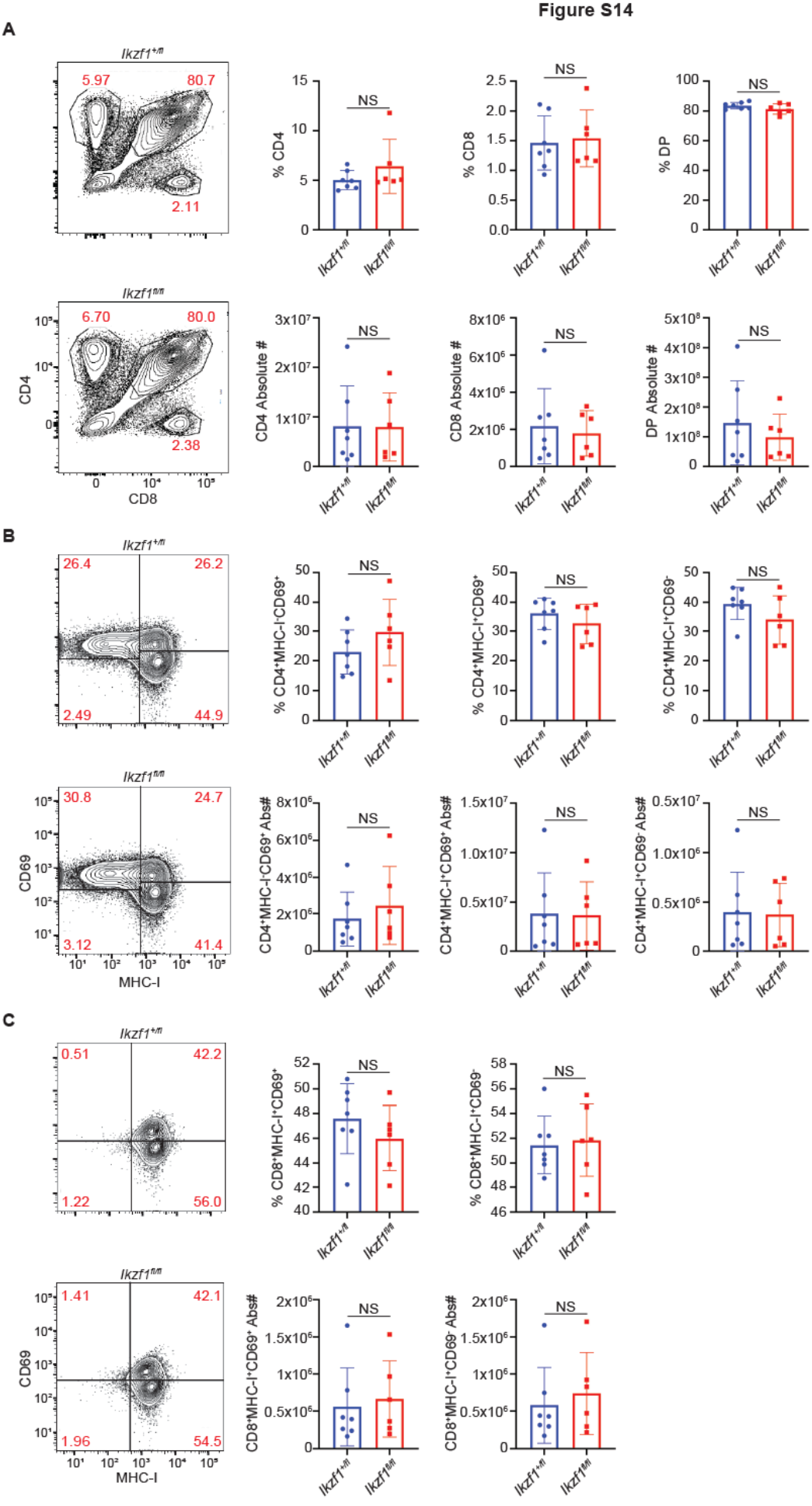
A
Ikzf1+/fl
5.97
80.7
2.11
Ikzf1fl/fl
6.70
80.0
2.38
CD4
CD8
% CD4
% CD8
% DP
CD4 Absolute #
CD8 Absolute #
DP Absolute #
NS
B
26.4
26.2
2.49
44.9
30.8
24.7
3.12
41.4
CD69
MHC-I
% CD4+MHC-I-CD69+
% CD4+MHC-I+CD69+
% CD4+MHC-I+CD69-
CD4+MHC-I-CD69+ Abs#
CD4+MHC-I+CD69+ Abs#
CD4+MHC-I+CD69- Abs#
C
0.51
42.2
1.22
56.0
1.41
42.1
1.96
54.5
% CD8+MHC-I+CD69+
% CD8+MHC-I+CD69-
CD8+MHC-I+CD69+ Abs#
CD8+MHC-I+CD69- Abs#

Fig. S14 – Deletion of *Ikzf1* in mTECs does not alter T cell development. (A) Flow cytometry plots (left) and counts (right) of thymocyte subsets from *Foxn1*-Cre/*Ikzf1*$^{+/fl}$ (*Ikzf1*$^{+/fl}$) and *Foxn1*-Cre/*Ikzf1*$^{fl/fl}$ (*Ikzf1*$^{fl/fl}$) mice. (n = 6-7 mice per genotype). **(B and C)** Flow cytometry plots (left) and counts (right) of CD69^{+}/MHC-I^{-} semi-mature (SM), CD69^{+}/MHC-I^{+} mature 1 (M1), and CD69^{-}/MHC-I^{+} mature 2 (M2), **(B)** SP CD4^{+} T cells and **(C)** SP CD8^{+} T cells. (n = 6-7 mice per genotype). **(A-C)** In graphs, the bar corresponds to the mean, with error bars showing +/- SD of values shown, and each data point represents an individual mouse. **(A-C)** Statistical significance was determined using Student's T-test. NS = not significant.

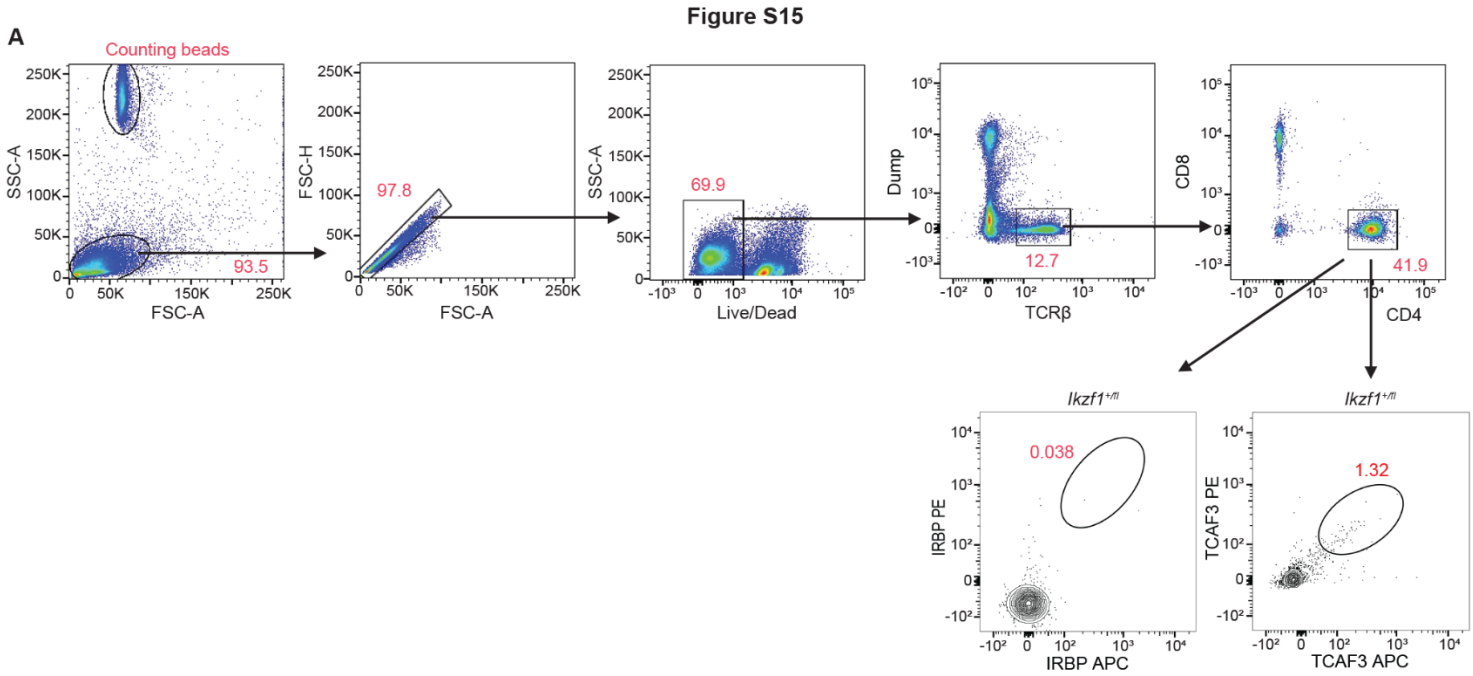

Fig. S15 – Gating strategy for IRBP and TCAF3 tetramer staining. (A) Representative gating strategy used for flow cytometry analysis of TCRβ^{+}CD4^{+}CD8^{-}IRBP^{+} and TCRβ^{+}CD4^{+}CD8^{-}TCAF3^{+} T cells from immunized *Foxn1*-Cre(+)/*Ikzf1*$^{+/fl}$ (*Ikzf1*$^{+/fl}$) mice.

Supplementary Table 1 – Resource Table.

Antibodies	Source	Clone/Tetramer Sequence	Used for
M2 antibody to Flag	Sigma	F1082	Co-IP/Western Blot
HRP-conjugated M2 anti-Flag	Sigma	A8592	Co-IP/Western Blot
HRP-conjugated anti-HA	Roche	12CA5	Co-IP/Western Blot
Anti-LaminB	Abcam	ab65986	Co-IP/Western Blot
HRP-conjugated donkey anti-rabbit	Jackson ImmunoResearch	711-035-152	Co-IP/Western Blot
A647-conjugated Krt10	Abcam	EP1607IHCY	Immunofluorescence
A488-conjugated DCLK1	Abcam	EPR6085	Immunofluorescence
e660-conjugated Aire	eBiosciences	clone 5H12	Immunofluorescence
A488-conjugated- Krt5	Abcam	EP1601Y	Immunofluorescence
Krt8 (Rabbit polyclonal to KRT8	Abcam	ab59400	Immunofluorescence
Rabbit polyclonal RFP antibody pre-adsorbed	Rockland	Cat. 600-401-379	Immunofluorescence
A488-conjugated Goat anti-Rabbit IgG (H+L) secondary antibody	Life Technologies	A-11008	Immunofluorescence
A647-conjugated goat anti-Rabbit IgG (H+L) secondary antibody	Thermo Scientific	A-21244	Immunofluorescence
Ikaros rabbit polyclonal targeting the N-terminus	gift to HS from Stephen T. Smale Lab, UCLA	-	Immunofluorescence
Rabbit monoclonal to DCLK1	Abcam	ab109029	Immunohistochemistry
Rabbit polyclonal to Biotin	Abcam	ab1227	Immunohistochemistry
LIVE/DEAD Fixable Blue Dead Cell Stain Kit	Thermo Fisher Scientific	Cat. L23105	Flow cytometry
PerCPCy5.5-conjugated CD8	BioLegend	SK1	Flow cytometry
PerCPCy5.5-conjugated CD44	Tonbo Biosciences	IM7	Flow cytometry
PerCP-conjugated CD45	Invitrogen	30-F11	Flow cytometry
BUV737-conjugated CD8a	BD Biosciences	53-6.7	Flow cytometry
Pacific Blue-conjugated CD19	BioLegend	6D5	Flow cytometry
Alexa Fluor e450-conjugated CD11B	Thermo Fisher Scientific	M1/70	Flow cytometry
BV421-conjugated F4/80	BioLegend	BM8	Flow cytometry
BV421-conjugated CD11c	BioLegend	N418	Flow cytometry
BUV737-conjugated CD11c	BD Biosciences	HL3	Flow cytometry
BV605-conjugated CD45	BD Biosciences	30 F11	Flow cytometry

Alexa Fluor e450-conjugated MHC-II I-Ab	Thermo Fisher Scientific	AF6-120.1	Flow cytometry
BV605-conjugated CD8	BD Biosciences	SK1	Flow cytometry
PE-Cy7-conjugated CD4	Tonbo Biosciences	RM4-5	Flow cytometry
PE-Cy7-conjugated CD45	Invitrogen	30-F11	Flow cytometry
PECy7-conjugated CD11c	Tonbo Biosciences	N418	Flow cytometry
PE-conjugated CD62L	Tonbo Biosciences	MEL-14	Flow cytometry
PE-conjugated CD44	BioLegend	IM7	Flow cytometry
PE-conjugated Ly51	BioLegend	6C3	Flow cytometry
PE-conjugated FOXP3	eBioscience	FJK-16s	Flow cytometry
PE-conjugated MHCI	eBioscience	AF6-88.5.5.3	Flow cytometry
PE-conjugated RORg	eBioscience	B2D	Flow cytometry
FITC-conjugated Foxp3	Invitrogen	FJK-16s	Flow cytometry
FITC-conjugated Ly51	BioLegend	6C3	Flow cytometry
FITC-conjugated CD69	Thermo Fisher Scientific	CH/4	Flow cytometry
A488-conjugated EOMES	Invitrogen	Dan11mag	Flow cytometry
A488-conjugated Aire	Thermo Fisher Scientific	5H12	Flow cytometry
A488-conjugated DCLK1	Abcam	EPR6085	Flow cytometry
A488-conjugated PLZF	eBioscience	Mags.21F7	Flow cytometry
APC-conjugated CD25	Tonbo	PC61.5	Flow cytometry
APC-conjugated MHC-II I-Ab	eBioscience	AF6-120.1	Flow cytometry
APC-conjugated Ikaros	BioLegend	2A9/Ikaros	Flow cytometry
A647-conjugated KRT10	Abcam	EP1607IHCY	Flow cytometry
Alexa Fluor e660-conjugated AIRE	eBioscience	5H12	Flow cytometry
APCCy7-conjugated EPCAM	BioLegend	G8.8	Flow cytometry
APCe780-conjugated TCRb	eBioscience	H57-597	Flow cytometry
Mouse CCL21/6Ckine Antibody	R&D Systems	MAB457	Flow cytometry
Rabbit polyclonal RFP antibody pre-adsorbed	Rockland	Cat. 600-401-379	Flow cytometry
PE-conjugated L1CAM	Bio-Techne	555	Flow cytometry
PE-conjugated Glycoprotein 2	MBL Life Science	2F11-C8	Flow cytometry
Alexa Fluor 647-conjugated Ki67	BD Pharmingen	B56	Flow cytometry
Alexa Fluor A488-conjugated UEA1	VWR	Cat. 10360-710	Flow cytometry
Donkey anti-goat IgG (H+L) secondary Antibody PE	Invitrogen	Cat. PA1-29953	Flow cytometry

PE-labeled tetramer for IRBP	NIH Tetramer Facility	QTWEGSGVLPCVG	Tetramer staining
APC-labeled tetramer for IRBP	NIH Tetramer Facility	QTWEGSGVLPCVG	Tetramer staining
PE-labeled tetramer for TCAF3	NIH Tetramer Facility	THYKAPWGELATD	Tetramer staining
APC-labeled tetramer for TCAF3	NIH Tetramer Facility	THYKAPWGELATD	Tetramer staining
BV421-labeled tetramer for CD1d	NIH Tetramer Facility	PBS-57	Tetramer staining